

# SYNTHETIC SYNCHROTRON EMISSION MAPS FROM MHD MODELS FOR THE JET OF M87

J. GRACIA

Dublin Institute for Advanced Studies, 31 Fitzwilliam Place, Dublin 2, Ireland

N. VLAHAKIS

IASA and Section of Astrophysics, Astronomy and Mechanics, Department of Physics, University of Athens, Panepistimiopolis, GR-157 84 Zografos, Athens, Greece

I. AGUDO

Instituto de Astrofísica de Andalucía (CSIC), Apartado 3004, E-18080 Granada, Spain

K. TSINGANOS

IASA and Section of Astrophysics, Astronomy and Mechanics, Department of Physics, University of Athens, Panepistimiopolis, GR-157 84 Zografos, Athens, Greece

AND

S. V. BOGOVALOV

Moscow Engineering Physics Institute (State University), Kashirskoje shosse 31, 115409 Moscow, Russia  
*Draft version November 9, 2018*

## ABSTRACT

We present self-consistent global, steady-state MHD models and synthetic optically thin synchrotron emission maps for the jet of M87. The model consist of two distinct zones: an inner relativistic outflow, which we identify with the observed jet, and an outer cold disk-wind. While the former does not self-collimate efficiently due to its high effective inertia, the latter fulfills all the conditions for efficient collimation by the magneto-centrifugal mechanism. Given the right balance between the effective inertia of the inner flow and the collimation efficiency of the outer disk wind, the relativistic flow is magnetically confined into a well collimated beam and matches the measurements of the opening angle of M87 over several orders of magnitude in spatial extent. The synthetic synchrotron maps reproduce the morphological structure of the jet of M87, i.e. center-bright profiles near the core and limb-bright profiles away from the core. At the same time, they also show a local increase of brightness at some distance along the axis associated to a recollimation shock in the MHD model. Its location coincides with the position of the optical knot HST-1. In addition our best fitting model is consistent with a number of observational constraints such as the magnetic field in the knot HST-1, and the jet-to-counterjet brightness ratio.

*Subject headings:* MHD – methods: numerical – radio continuum: galaxies – galaxies: jets – galaxies: individual: M87

## 1. INTRODUCTION

Since its discovery by Curtis (1918) the jet of M87 is the classical prototype for extragalactic jets. Due to its proximity at 16 Mpc (Whitmore et al. 1995; Macri et al. 1999; Tonry et al. 2001) M87 is one of the closest radio galaxies, which allows present VLBI instruments to resolve the transversal structure of the jet. Therefore, it is an ideal candidate for testing specific jet formation mechanisms. The jet and its hot spots have been systematically studied across the electromagnetic spectrum from the radio to X-rays, both, with ground-based observations and from satellites (for a review see e.g. Biretta 1996). The initial opening angle is approximately  $60^\circ$  on scales of about 0.04 pc and decreases rapidly until reaching  $10^\circ$  at a distance of 4 pc from the core (Biretta et al. 2002). These observations suggest that the jet of M87 is rather slowly collimated across a length of several parsec.

The prevailing paradigm for jet formation and

collimation is magnetic self-collimation by the Blandford & Payne (1982) mechanism. This view is supported by observations, which are consistent with the presence of a non-vanishing toroidal magnetic field component (Asada et al. 2002, 2008; Gabuzda et al. 2004; Zavala & Taylor 2005; Gómez et al. 2008). However, relativistic effects have been shown to decrease the collimation efficiency, i.e. for a given magnetic field configuration at the base of the jet (or rotator efficiency), the fraction of total mass- and magnetic flux that is asymptotically cylindrically collimated is lower for a relativistic flow than for a non-relativistic flow (Bogovalov & Tsinganos 1999; Tsinganos & Bogovalov 2000). Not only is the mass flux fraction lower, but the final opening angle is larger for relativistic outflows due to the decollimating effect of the electric field and the effective inertia of the plasma (Bogovalov 2001), which both counter-act the pinching by the toroidal magnetic field. However, this is strictly true only for initially radial magnetic field structures, as opposed to extended

magnetic field configurations like disk-winds. See, e.g. Fendt & Memola (2001); Vlahakis & Königl (2004); Komissarov et al. (2007) for efficiently collimating MHD disk-wind models.

In a series of papers Gracia et al. (2005); Tsinganos & Bogovalov (2005, 2002) suggested a steady-state two-component MHD model. The model consists of an inner relativistic outflow, which is identified with the observed jet, and an outer non-relativistic disk-wind. While the inner relativistic jet is not expected to collimate well through magnetic self-collimation, the very same process operates efficiently in the outer non-relativistic disk-wind. It is expected, that at least for a part of the available parameter space, collimation in the outer disk-wind is so efficient, that it might resist the decollimating inertia of the inner relativistic plasma and channel the jet into a narrowly confined beam. Gracia et al. (2005) have shown, that such two-component models could easily account for the narrow appearance of the beam of extragalactic jets by reproducing the observational measurement of the opening angle distribution as a function of angular distance from the core by Biretta et al. (2002). Since in these models the jet, i.e. the relativistic inner outflow, is strictly speaking not magnetically self-collimated, but rather confined by the outer disk-wind, the authors prefer to talk of collimation by magnetic confinement.

However, Gracia et al. (2005) could not fit the opening angle distribution with a unique MHD model. Instead various sets of parameters reproduce the observations with similar accuracy.

In deriving the opening angle of their model, Gracia et al. (2005) made a simplifying but crucial assumption. They identified the observed jet with the inner relativistic outflow of their two-component model. More specifically, the boundary of the jet was assumed to coincide with the shape of a specific fieldline  $\Psi_\alpha$ , the one fieldline, which separates the relativistic inner region from the non-relativistic outer disk-wind at the base, or the launching surface, of the outflow. So, the observed opening angle was strictly speaking fitted by the shape of a single magnetic fieldline.

However, observations do not measure the plasma state directly, i.e. in terms of velocity, temperature or magnetic field strength. Instead, they register photon flux as a function of position on the plane of the sky. As such, from an observational point of view, the width of the jet is defined by the emission dropping below the detection limit or a small fraction of the luminosity of the ridge line of the jet. So the question is how well did Gracia et al. (2005) measure the width of the jet in terms of observational quantities? Or more generally – Do MHD models explain the appearance of AGN jets? The purpose of this paper is to answer exactly this question by adopting the point of view of an observer. Assuming, that the main radiation mechanism is synchrotron emission, we translate the steady-state MHD model into a synthetic emission map and measure the width of the jet using only these data.

The outline of the paper is as follows. In the following section 2 we summarize the two-component MHD model for extragalactic jets and discuss some of its properties relevant to this work. In section 3 we present compact expressions for the calculation of synchrotron emission

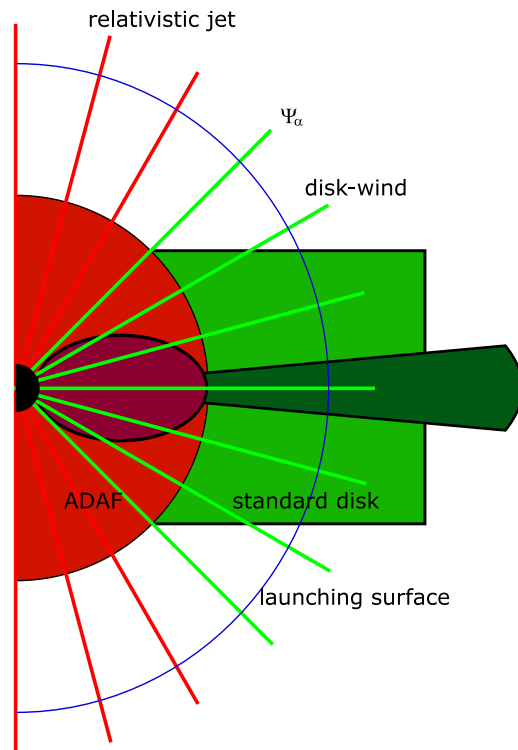


FIG. 1.— Illustrative sketch of the model (see text).

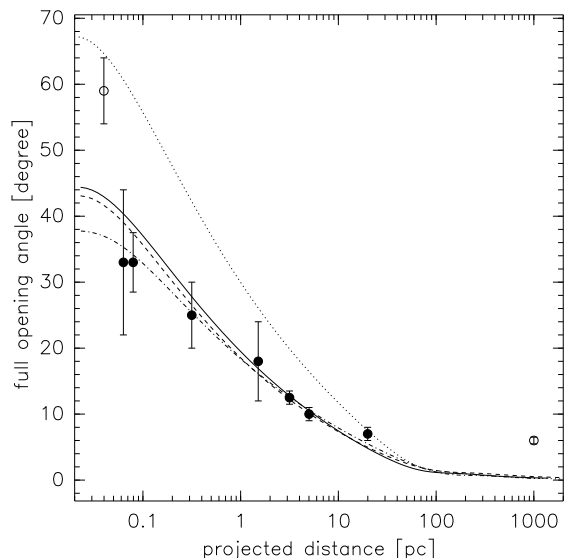


FIG. 2.— Comparison of the opening angle calculated from our MHD models and the observational data for M87. The lines show opening angle profiles as given by the separating fieldline  $\Psi_\alpha$  for model A (solid line), i.e. the best model, and model D (dot-dashed), which best reproduces the data based on  $\Psi_\alpha$ . The models B (dashed) and C (dotted) are shown for completeness. The data points marked by filled circles were taken into account in the fitting procedure. The innermost and outermost measurement (open circles) were disregarded.

and apply these to our numerical MHD models for the jet of M87. Finally, we discuss our results and draw some conclusions.

## 2. MHD MODEL

TABLE 1  
PARAMETERS AND DESCRIPTION OF MODELS.

name	$\alpha$ [°]	$T_i$ [mc <sup>2</sup> ]	$\Gamma_i$	$\omega_i$ [ $r_g/c$ ]	$\Gamma_d$	$B_0$	remarks
model A	16.15	2.85	2.74	3.0	1.02	1.1	best overall model
model B	14.45	3.0	2.74	3.0	1.02	0.9	best fit to opening angle based on synchrotron map
model C	24.0	3.0	1.8	2.7	1.02	1.0	highest limb-brightening and brightest knot HST-1
model D	14.4	3.45	3.26	3.0	1.01	1.27	best fit to opening angle based on field line

The mass-flux rate of  $10^{24}$  gs<sup>-1</sup> is a parameter common to all models.

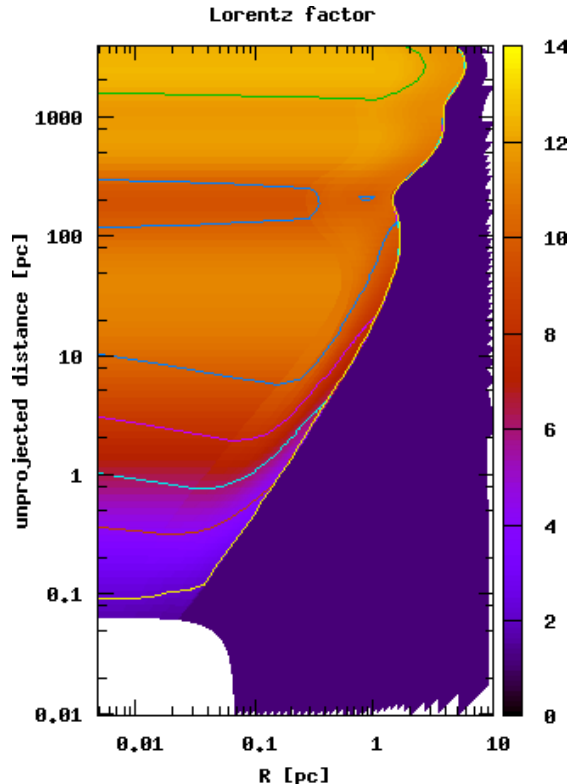


FIG. 3.— Lorentz factor along the flow for model A. Contour levels are shown at  $\Gamma = 2, 4, \dots, 12$ . The relativistic inner jet initially has Lorentz factors  $\Gamma \sim 2 - 3$ , but accelerates up to  $\Gamma \sim 10 - 12$ . Strong gradients may be seen across the jet and near the recollimation shock, if present.

We adopt the model and notation of Gracia et al. (2005) and refer the reader to that paper for details. A simple illustration of the model is shown in Figure 1. It consist of two distinct zones; an inner outflow, which is dominated by relativistic dynamics, and an outer non-relativistic outflow. Both outflows originate from a spherical launching surface located at a distance  $r_0$  from the black hole. The launching surface is threaded by a helical magnetic field; the poloidal component is initially perpendicular to the launching surface. The two zones are separated by a specific fieldline  $\Psi_\alpha$ , where  $2\alpha$  is the initial angular width, or opening angle, of the inner relativistic outflow. In the following, we will refer to these two distinct zones by relativistic jet and (non-relativistic) disk-wind, respectively.

This two-component model is motivated by a similar two-component structure of the underlying accretion flow consisting of an outer standard disk (Shakura & Sunyaev 1973) and an inner hot plasma, which could be either an advection dominated accretion flow (Narayan & Yi 1994; Peitz & Appl 1997; Gracia et al. 2003), or the fi-

nal plunging region near the black hole, where relativistic dynamics dominates through, e.g., frame-dragging, or the Blandford-Znajek process.

We impose two different sets of boundary conditions in the two distinct zones along the launching surface. If the launching surface is located beyond the fast magnetosonic surface, i.e. in the hyperbolic MHD regime, the steady-state problem reduces to an initial value Cauchy-type problem and the steady-state equations can be integrated directly in terms of conserved integrals of motion as described in Tsinganos & Bogovalov (2002). We stress, that beyond the launching surface we solve the axisymmetric steady-state problem self-consistently, including the magnetic field structure, as a function of the boundary values alone. However, we do not solve the problem inside the launching surface, which is a much more complicated exercise. A self-consistent solution of the full problem needs to take into account the dynamics of the accretion flow, something which is beyond the scope of this paper.

This procedure yields a set of quantities as a function of space in the comoving frame of the jet. The separating fieldline  $\Psi_\alpha$  perfectly divides the relativistic from the non-relativistic outflow. Inside of  $\Psi_\alpha$  the plasma is highly relativistic, both in terms of its bulk Lorentz factor,  $\Gamma \gg 1$ , and of its thermal energy,  $T \geq mc^2$ , while outside the plasma is cold,  $T \ll mc^2$ , and moving at non-relativistic speeds,  $\Gamma = 1$ . Also, the magnetic field strength peaks close to the separating fieldline, where fieldlines (and poloidal flowlines) of the inner outflow are strongly compressed laterally and confined to a narrow sheet by the fieldlines of the outer disk-wind thus forming a natural interface between both zones.

Gracia et al. (2005) used the shape of the separating fieldline  $\Psi_\alpha$  to fit the observed opening angle (Biretta et al. 2002) as a function of distance from the core, however, without taking into account projection effects, i.e. they assumed implicitly, that the jet of M87 was in the plane of the sky. There is an on-going discussion on the inclination angle of the M87 jet (see e.g. Owen et al. 1989; Reid et al. 1989; Biretta et al. 1999; Ly et al. 2007). In this paper we assume, that the jet of M87 is oriented at an angle  $\theta_{\text{los}} = 40^\circ$  from the line-of-sight as a compromise of values discussed in the literature.

Unfortunately, the parameter space of the MHD model is degenerated in the sense, that very different sets of parameters yield equally good fits or even almost identical opening angle distributions. Then, in order to further constrain the model parameters we shall invoke the radiation signatures of each model and compare them with the corresponding observations. In this way, we may pin down a small number of acceptable models which simultaneously satisfy the constraints of the MHD model and

also reproduce the observed distribution of the emitted radiation.

We have run 2600 axisymmetric steady-state MHD models and calculated synthetic synchrotron maps for them. Here we discuss the four models that evaluate best under different criteria. See table 1 for their parameters. Figure 2 compares the opening angle as defined by the separating fieldline  $\Psi_\alpha$ , projected under an angle of  $\theta_{\text{los}} = 40^\circ$ , with the observational measurements. Note that all our models fail to fit the jet width at large distances close to the optical knot A at  $\sim 900$  pc and also at small distances close to the jet's origin, where there are some uncertainties, as is discussed in the last section of the paper. Models with large initial opening angle matching the first data point as e.g. model C, have difficulties reproducing the opening angle distribution. It is in general very difficult to make the curve more concave. Models with initial opening angles falling slightly short of the measured value (as models A, B, and D) may easily reproduce the rest of the measurement and yield quite good fits. The quality of agreement between the observed opening angle distribution and the theoretical curve is measured by a simple  $\chi^2$ , i.e. the sum of squares of the difference over the available observational data points. Model D best fits the opening angle at  $\chi^2 = 2.9$ , but does not reproduce the morphological structure of the radiomaps particularly well, as will be discussed in the next section. However, the overall best model A reproduces the morphological structure and still fits the opening angle data reasonably well with  $\chi^2 = 7.8$ . Note, that both models show a clear kink at  $\sim 100$  pc due to recollimation towards the axis.

Typically, models that fit the observed opening angle well are moderately relativistic, both in terms of the initial outflow velocity  $\Gamma_j \sim 2 - 3$  and the initial plasma internal energy  $T_j \sim 3mc^2$ . In these models the plasma velocity increases along the flow to values up to  $\Gamma \sim 5 - 10$ . However, the plasma may decelerate and reaccelerate sharply at the recollimation shock. Strong gradients of the plasma velocity may generally be present across the jet, as seen in Figure. 3. It is therefore very difficult to assign a *typical* Lorentz factor to the whole jet.

### 3. SYNCHROTRON MAPS

#### 3.1. Calculation of synchrotron maps

The calculation of the radio emissivity is done according the relativistic generalization of expressions presented by Laing (1981) and Pacholczyk (1970). It is assumed that the radiating region is optically thin with a uniform and isotropic distribution of electrons

$$N'(E') \propto E'^{-(2\alpha_e+1)} \quad (1)$$

giving rise to radiation with a spectral index  $\alpha_e=1$ , i.e.,  $S'_\nu \propto \nu'^{-\alpha_e}$ . Note, that primed quantities are measured in the comoving frame of the plasma, while unprimed quantities refer to the lab frame or are independent of the frame of reference.

We assume further, that the fraction of electron number density to proton number density is constant throughout the emitting volume. Then the number density of electrons  $n_e = \int N(E)dE$  is proportional to the density of the plasma, i.e.  $n_e \propto \rho$  in every frame of reference.

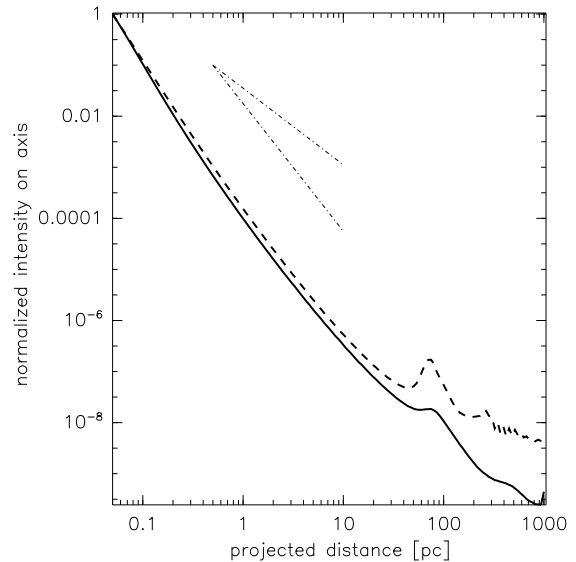


FIG. 4.— Comparison of the normalized synchrotron intensity along the jet axis calculated from model A (*solid lines*) and model C (*dashed lines*), respectively. The dashed lines indicate power-laws with index -1.5 and -2.5, respectively.

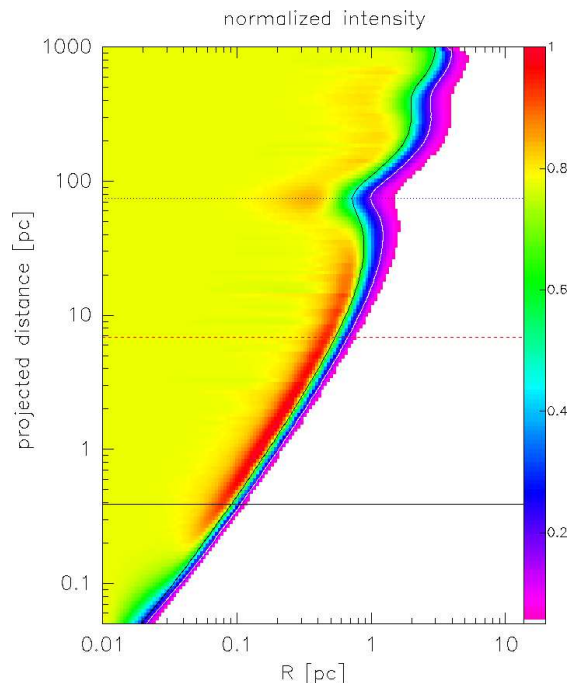


FIG. 5.— Convolved synthetic synchrotron map. To increase contrast, the map has been divided by the trend along the jet axis (Figure 4). The two lines near the edge of the jet indicate the jet width as defined by the separating fieldline (*inner black line*) and the HWQM of the map (*outer white line*). The three horizontal lines indicate the position of cuts across the jet shown in Figure 6.

If the radiating plasma moves at relativistic speeds  $\mathbf{v}$ , i.e.  $\Gamma = 1/(1 - \beta^2)^{1/2} \gg 1$  with  $\beta = v/c$ , it is convenient to evaluate the synchrotron emission in the comoving frame  $\Sigma'$ , instead of the lab- or observer frame  $\Sigma$ . Note however, that the velocity of the comoving frame is not constant within the emitting region, unless the velocity field  $\mathbf{v}$  is homogeneous, which is not true in our model. The synchrotron emissivity in the comoving frame  $\epsilon'$  is related to the magnitude of the magnetic field perpen-

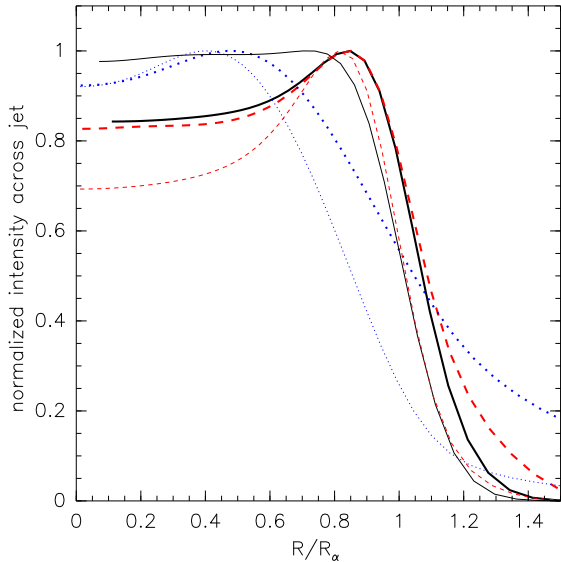


FIG. 6.— Comparison of the normalized synchrotron intensity across the jet beam. The overall best model A is indicated by heavy thick lines. For comparison model C, which has the most pronounced limb-brightening, is shown with thin lines. We plotted cuts across the jet beam at three different positions along the jet, i.e. close to the core (*solid/black line*), at intermediate distance (*dashed/red line*), and at large distance (*dotted/blue line*). See Figure 5 for the location of the cuts. The lateral coordinate is normalized to the width of the jet  $R_\alpha$  as defined by the separating fieldline  $\Psi_\alpha$  and the intensity is normalized to unity at the maximum.

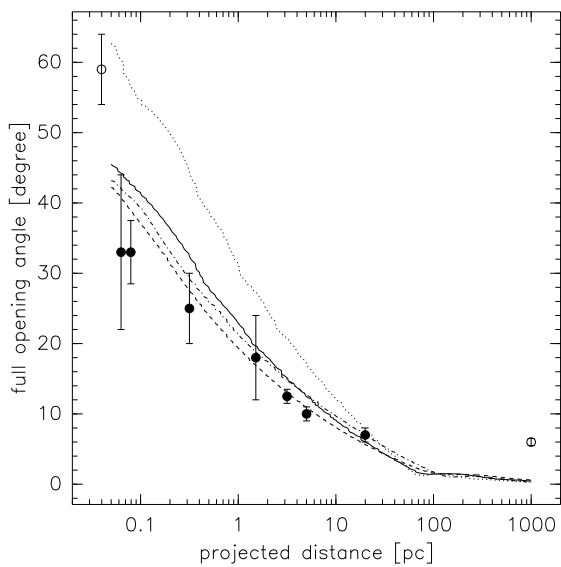


FIG. 7.— Comparison of the opening angle calculated from synthetic maps and the observational data for M87. The lines show opening angle profiles as given by the HWQM contour  $R_{\text{map}}$  of the overall best model A (*solid line*), and model B (*dashed line*) which fits the opening angle data best. Models C (*dotted*) and D (*dot-dashed*) are shown for comparison. Various symbols represent observational measurements. The data points marked by *filled circles* were taken into account in the fitting procedure. The innermost and outermost measurement (*open circles*) were disregarded as explained in the text.

dicular to the line-of-sight and the electron density as

$$\epsilon' \propto \rho' |\mathbf{B}' \times \hat{\mathbf{n}}'_{\text{los}}|^{\alpha_e + 1}, \quad (2)$$

where  $\rho'$ ,  $\mathbf{B}'$  and  $\hat{\mathbf{n}}'_{\text{los}}$  are the electron density, magnetic field and line-of-sight unit vector in the comoving. These are given in terms of the observers frame quantities through the Lorentz-transformations as,

$$\rho' = \rho/\Gamma, \quad (3)$$

$$\mathbf{B}' = \frac{1}{\Gamma} \mathbf{B} + \frac{\Gamma}{\Gamma + 1} \frac{\mathbf{v}}{c^2} (\mathbf{v} \cdot \mathbf{B}), \quad \mathbf{E}' = 0 \quad (4)$$

$$\hat{\mathbf{n}}'_{\text{los}} = \mathcal{D} \hat{\mathbf{n}}_{\text{los}} - (\mathcal{D} + 1) \frac{\Gamma}{\Gamma + 1} \frac{\mathbf{v}}{c}. \quad (5)$$

We have introduced the Doppler factor  $\mathcal{D} = (\Gamma(1 - \mathbf{v} \cdot \hat{\mathbf{n}}_{\text{los}}/c))^{-1}$  for a compact notation and exploited the fact, that in ideal MHD Ohm's law holds as  $\mathbf{E} = -\mathbf{v} \times \mathbf{B}$  in both frames of reference.

The emissivity in the lab frame  $\epsilon$  appears Doppler-boosted as

$$\epsilon = \mathcal{D}^{\alpha_e + 2} \epsilon'. \quad (6)$$

The amount of relativistic beaming strongly depends on the line-of-sight angle, i.e. the angle between the jet axis and the direction to the observer, which we fix to  $\theta_{\text{los}} = 40^\circ$ . Finally, the flux in the plane of the sky,  $I$ , is given by integration along the line-of-sight

$$I = \int \epsilon dl_{\text{los}}. \quad (7)$$

The synthetic synchrotron maps are convolved with a Gaussian beam to qualitatively match the finite resolution of observed maps. However, since our synthetic maps span more than four orders of magnitude in distance from the core, the width of the Gaussian beam is not kept constant. Typical radiomaps have a spatial resolution corresponding to a couple of observing beams across the width of the jet. We therefore use at each distance along the jet a Gaussian convolution kernel of 1-sigma width equal to a tenth of the jet radius at that distance, i.e.  $\sigma(Z) = R_\alpha(Z)/10$ .

The measurements of the opening angle collected by Biretta et al. (2002) typically define the jet radius at distance  $Z$  as the *half-width at quarter-maximum* (HWQM) for the emission across the jet. We adopt this definition and refer to it as the jet width of the radiomap  $2R_{\text{map}}$ , with

$$I(R_{\text{map}}, Z) = \max(I(R, Z))/4. \quad (8)$$

### 3.2. The best model

The synthetic synchrotron emission maps shall qualitatively reproduce two observational constraints: (i) the opening angle defined through HWQM (half-width at quarter-maximum) in terms of small  $\chi^2$  values, and (ii) the pronounced limb-brightening in terms of small values for the mean intensity on the axis over intensity on the limb, i.e.  $\langle I_{\text{axis}}/I_{\text{limb}} \rangle$ . As a secondary criterion, we favor models showing some degree of enhanced emission close to the nominal position of HST-1 at 70 pc.

We calculated synthetic synchrotron emission maps and evaluated them according to our two criteria. For each of the two criteria we assigned a score between 0..1

from a sorted list of values for  $\chi^2$  and  $\langle I_{\text{axis}}/I_{\text{limb}} \rangle$ , respectively, and added those to obtain the total score. A few formally high scoring models were discarded because they did not show clear sign of increased brightness at distances 70-200 pc, that could be identified with the knot HST-1. The first model satisfying all criteria will be referred to as *the best model* or simply *model A*.

The jet in the best model A is launched with a bulk velocity of  $\Gamma_j = 2.74$  and temperature  $T = 2.85 mc^2$ . The separating field line threads the launching surface radially at an angle  $\alpha = 16^\circ$  with an angular velocity  $\omega_j = 3 r_g/c$ . The outer cold disk-wind is launched with velocity  $\Gamma_d = 1.02$ .

For the best model A we plotted spatial 2-dimensional synthetic synchrotron emission maps (Figure 5), the intensity measured on the jet axis as a function of distance from the core (Figure 4), and the intensity profiles across the jet at various positions along the jet axis (Figure 6).

In Figure 4 we plot the trend along the axis for the best model A and compare it with model C, which shows the highest local brightness enhancement at the position of HST-1 in our sample. The intensity along the axis is well described by a power-law in projected distance. Both models have similar power-law indices  $\sim -2.5$ . The model jets dim out faster than the observed jet whose power-law index can be estimated to  $\sim -1.5$  from the contrast of several published intensity maps. However, this discrepancy is not surprising as our model does not take into account any micro-physics in order to re-energize the electron distribution. Both models show a rise of luminosity around 70 pc over the local power-law by a factor of  $\sim 3$  and  $\sim 10$ , respectively. The location of this bright spot coincides with the location of strong recollimation shocks, where density and magnetic field strength increase.

Figure 5 shows the synthetic synchrotron map. In order to increase the contrast we divided the map by the trend along the jet axis, i.e.  $I(R, Z)/I(0, Z)$ . The jet beam is well defined, showing large opening angles close to the core and becoming almost conical at large distance. At the position of the recollimation shock the jet width decreases and forms a visible neck.

The synthetic synchrotron maps show strong gradients of intensity across the jet. These are more clearly visible in Figure 6, where cuts across the jet are shown. For comparison we show also profiles for model C which has the most pronounced limb-brightening.

The best model A shows limb-brightening already at a distance  $\sim 0.2$  pc from the core. In the limb-bright region  $\langle I_{\text{axis}}/I_{\text{limb}} \rangle = 0.76$  on average before convolution. After convolution, the ratio rises to typically 0.85. Model C bifurcates at  $\sim 0.5$  pc and has  $\langle I_{\text{axis}}/I_{\text{limb}} \rangle = 0.67$  and 0.80 before and after convolution, respectively. These values agree with those from observations by Ly et al. (2007)  $\sim 0.63$ , Kovalev (2008)  $\sim 0.6$ , and Kovalev et al. (2007, and private communication) 0.6 – 0.8, depending on jet region and resolution. We note however, that the limb-brightness, as well as the bifurcation distance depend on the details of convolution as discussed later on.

Figure 7 compares the opening angle derived from the synthetic maps  $R_{\text{map}}$  with the observations. Model B fits the observations best with  $\chi^2 = 5.7$ , but fails to reproduce the limb-brightening. The best model A has

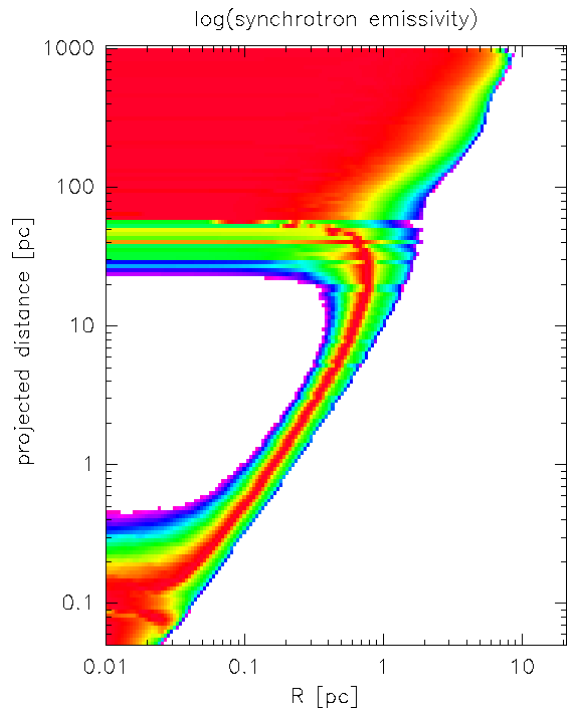


FIG. 8.— Synchrotron emissivity in the mid plane of the jet. To increase contrast we normalized each row at distance  $Z$  by the maximum emissivity across the jet at that particular distance. Close to the core the whole jet body contributes to the total emission along the line-of-sight. Further down the flow, most of the synchrotron emission originates from a thin shell at the outer edge of the jet, causing the bifurcation of the jet from center-bright to limb-bright.

$\chi^2 = 14.6$ , which we consider acceptable, in particular, if one considers the figure.

Finally, we compare the width of the jet from the MHD models,  $R_\alpha$ , with the jet width of the synthetic synchrotron maps,  $R_{\text{map}}$ . Both curves are superimposed on the synthetic map in Figure 5. For many models in our sample these two curves are virtually indistinguishable. However, for our overall best model, these two curves are noticeably different, even if they run almost parallel. For this particular model  $R_\alpha$  underestimates the opening angle by  $\sim 20\%$  for all the length of the jet, i.e.  $R_{\text{map}} \sim 1.2R_\alpha$ . For other models in our sample, the difference is typically not more than 30% – 40%.

### 3.3. The origin of limb-brightening

The synthetic emission map of the best model A in Figure 5 shows clear limb-brightening from a distance of  $\sim 0.5$  pc up to the location of the recollimation shock at  $\sim 70$  pc and to a lesser extent even beyond. This can be seen more clearly in Figure 8, which shows the synchrotron emissivity  $\epsilon'$  in the mid plane of the jet. It is worth noting, that close to the origin the whole jet body emits synchrotron radiation. Further down the jet – and certainly beyond 0.2 pc projected distance from the core – the emission is dominated by a thin shell at the outer edge of the jet, while the inner region close to the axis remains relative dark by a factor of more than a hundred. Within our model this is easily explained noting that the synchrotron emissivity equation (2) is roughly proportional to  $\rho' B'^2$ . Fieldlines within the relativistic jet start out radially from the launching surface, but are soon deflected by the outer cold disk wind. This leads

to strong concentration of magnetic flux, and therefore high field strength in a narrow region at the interface between both components of the MHD model. The simultaneously occurring increase of density plays only a minor role.

Further down the flow, at around 60 pc, the emissivity within the jet body increases again significantly and edge-brightening is less pronounced. This region coincides well with the location of the recollimation shock, where the topology of the magnetic field and the distribution of plasma across the jet change significantly again. Beyond the recollimation shock, the emissivity is almost homogeneous across the jet.

However, the full picture is more complicated than that, since the orientation of the highly non-homogeneous velocity field relative to the line-of-sight is at least equally important. Not only does the poloidal velocity vary from one magnetic flux surface to the next, but the jet plasma is also rotating. Together this makes the Doppler factor and the angle to the line-of-sight in the comoving frame highly variable even along the circumference of the emitting plasma shell. Cross sections perpendicular to the apparent axis of the jet reveal, that the emissivity along the line-of-sight may be highly asymmetric with respect to fore- and background halves of the jet.

#### 4. DISCUSSION

Limb-brightening strongly constrains the parameters of MHD models for the jet of M87. It is not only difficult to find parameters resulting in a pronounced limb-brightening in terms of low  $\langle I_{\text{axis}}/I_{\text{limb}} \rangle$ , but also reproducing the spatial extend of the limb-bright region. Depending on frequency and resolution, radiomaps for M87 show limb-brightening from large distances almost right down to the core (Cheung et al. 2007; Kovalev et al. 2007). However, the bifurcation distance, i.e. the location where the jet morphology transits from center-bright to limb-bright, seems to depend strongly on the frequency of a particular observation. It is not clear *a priori* to what extent this is due to intrinsic different emission properties at different observing frequencies, or due to spatial resolution effects. Y. Y. Kovalev (private communication) has performed an analysis of the deep 15 GHz VLBA image of the inner jet in M87 (Kovalev et al. 2007). The distance from the core at which the bifurcation becomes detectable changes from 5 mas at the original 15 GHz resolution to more than 100 mas for a tenfold larger beam corresponding to 1.5 GHz. We conclude, that variable resolution can in principle account for different bifurcation distances at different frequencies.

Limb-brightening is often explained by stratified jets consisting of a fast spine and a slow sheath (see e.g. Aloy et al. 2000; Ghisellini et al. 2005). In those models the slow sheath brightens up in comparison to the spine because of Doppler boosting into the  $1/\Gamma$  cone. For the given large line-of-sight angle of the M87 jet, the fast spine is seen from well outside of the Doppler-boosted cone and its emission deboosted. Here we suggest an alternative explanation for limb-brightening in AGN, in particular M87. In our model the limb brightens up due to the concentration of magnetic flux at the interface between the relativistic jet and the confining

non-relativistic disk-wind. The synchrotron emissivity is therefore already intrinsically higher in the comoving frame and limb-brightening does not rely on relativistic aberration alone. Incidentally, as seen in Figure 3 in our models the spine may at times be moving slower than plasma further out which will counteract limb-brightening for large inclination angles.

The exact value of the line-of-sight angle for the jet of M87 is still under debate. In this study we have assumed an angle  $\theta_{\text{los}} = 40^\circ$  which brings it into the upper end of the suggested range of values. In order to study the effect of the line-of-sight angle on limb-brightening we have calculated synthetic maps for model A under an angle  $\theta_{\text{los}} = 30^\circ$ . In comparison to the original map, the bifurcation distance moves out to 0.5 pc, limb-brightening is more pronounced, and the recollimation shock is brighter with regard to the trend along the axis. At the same time this obviously enlarges the apparent opening angle along the jet and brings the recollimation shock closer to the core in disagreement with observations. The simplest way to bring the opening angle curve back down and move the recollimation shock out, is to decrease the model's initial opening angle  $\alpha$ . However, models with lower  $\alpha$  tend to show weaker limb-brightening and dimmer recollimation shocks (if present at all). It may therefore be challenging to construct models that reproduce all criteria for smaller inclination angles.

Under the assumption that jet and counterjet are intrinsically identical, one can in principle constrain the inclination angle by measuring the jet-to-counterjet brightness ratio  $I_+/I_-$  given by

$$I_+/I_- = \left( \frac{1 + \beta \cos \theta_{\text{los}}}{1 - \beta \cos \theta_{\text{los}}} \right)^{\alpha_e + 2}, \quad (9)$$

where  $\beta = v/c$  is the velocity in units of the speed of light and  $\alpha_e$  the electron distribution power-law index. Kovalev et al. (2007) estimated this ratio to be of the order 10 - 15, while Ly et al. (2007) measured  $I_+/I_- = 14.4$  and constrained the bulk flow velocity to  $\beta \sim 0.6 - 0.7$ . We calculated a synthetic synchrotron map for the best model A pointing in the opposite direction, i.e. the counterjet at  $\theta_{\text{los}} = 220^\circ$ , and estimated  $I_+/I_- \sim 13$  from the on-axis intensities close to the core on either side of it (see Fig 9). The agreement is remarkable, in particular taking into account, that one would naively expect a much higher value ( $> 200$ ) from the model's initial Lorentz factor  $\Gamma_j = 2,74$ , i.e.  $\beta_j = 0.93$ , given in table 1. However, eq. (9) assumes a homogeneous velocity field along the axis and identical intrinsic emissivities on either side of the core. Stratification of the jet beam and rotation of the plasma about the axis, as is the case in our models, can therefore lead to serious misinterpretation if not taken into account.

While fitting the opening angle to the observational measurements collected by Biretta et al. (2002), we disregarded the outermost data point close to the optical knot A at 900 pc. All our models fail to reproduce this measurement and disregarding it made the least-squares-fit more reliable and robust for the remaining data points. However, we argue, that at such large distances the interaction between the environment and the jet, which cannot be taken into account by our numerical MHD solver, begins to dominate the jet dynamics and thus

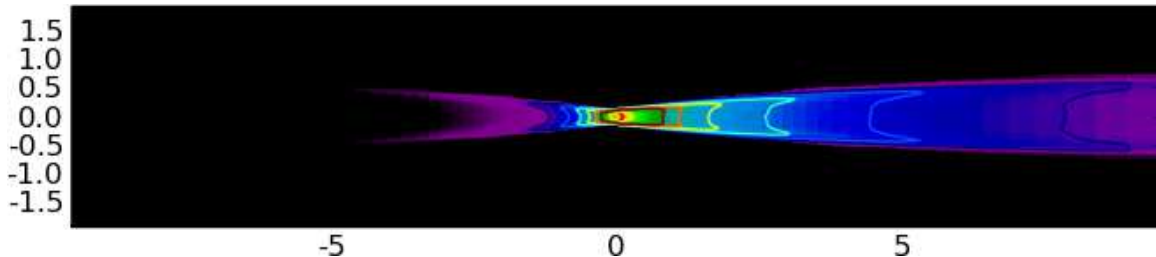


FIG. 9.— Synthetic synchrotron map for the inner jet of M87 including the counterjet convolved with a constant Gaussian beam of  $\sigma = 0.03\text{pc}$ . Unlike Fig 5 this map has not been divided by the trend along the axis, but shows the full dynamic intensity contrast of 50000 on a logarithmic scale. The contour lines are chosen as indicated on the colorbar in order to highlight the limb-brightening. The counterjet is under-luminous by factor of  $\sim 13$ . This map is meant to be compared to Fig 1 in Kovalev et al. (2007).

renders our model insufficient. We have also disregarded the innermost data point of  $60^\circ$ . This old measurement has been challenged recently. Ly et al. (2007) state that the opening angle at the jet base is larger than  $15^\circ$  and therefore consistent with Biretta et al. (2002) old measurement, but then interestingly continue to repeat arguments that it might be an overestimation. Maps presented by Krichbaum et al. (2008) and Walker et al. (2008) seem to leave room for smaller opening angles at the base. In general, the initial opening angle measured from our synthetic emission maps can easily be higher than  $40^\circ$ .

Most of our models that reproduce the measured opening angle as a function of distance as well as the limb-brightening, do at the same time exhibit a recollimation shock<sup>1</sup> showing some degree of locally enhanced emission. We identify this recollimation shock with the bright knot HST-1. In most of our models the emission at the bright knot does not increase by more than a factor of 10 compared to the general trend, while for the real HST-1 the increase in emission level is probably higher. However, this is not surprising, since our MHD model does not include any micro-physics as e.g. particle acceleration, that could be responsible for further enhancing the emission level. It is still noteworthy, that the conditions in the vicinity of the recollimation shock of the best model A, are similar to those postulated from SSC models in order to fit the TeV emission in M87. In particular Harris et al. (2003) recently presented a SSC model assuming, that the TeV emission was originating from HST-1. In our model the Doppler factor in the vicinity of the recollimation shock is rather low  $\mathcal{D} \sim 1 - 2$ . For those Doppler factors, Harris et al. (2003) calculated a magnetic field strength of  $B' = (13 - 3.7)\text{mG}$ , which matches very well  $B' \sim 10\text{mG}$  in our model.

## 5. SUMMARY AND CONCLUSIONS

We have calculated self-consistent global MHD models and synthetic optically thin synchrotron maps with the aim to reproduce the reported opening angle distribution as well as the morphological structure, in particular limb-brightening, of the jet of M87. We have applied different criteria to quantify the agreement between models and observations. All criteria can be satisfied to high degree by individual models in our database. However, no model does satisfy simultaneously all criteria exceedingly well.

<sup>1</sup> We also have a small range of models, that reproduces the opening angle without showing a strong recollimation shock (see Gracia et al. 2005, Figure 2), but those models do in general not show clear limb-brightening.

We identified a *best model* as compromise between the opening angle distribution and the high degree of limb-brightening. This model satisfactorily meets our criteria, but does not perform best in any single one.

Gracia et al. (2005) used the shape of the fieldline separating the two regions on the boundary surface to define the opening angle. As shown in this work, this particular fieldline and flux contours of synthetic maps are parallel for a wide range of models and distances along the jet. However, the first method may under-estimate the opening angle for some parameters by typically 30%.

The morphological structure across the jet can be reproduced in principle. A wide range of models show limb-brightening away from the core. The transition from center-bright to limb-bright, the bifurcation of the jet, generally occurs well below 1 pc projected distance. A quantitative comparison with specific observations, however, requires careful modeling of the convolving beam and may require including opacity effects, i.e. optically thick emission. Both effects are frequency dependent.

In our models limb-brightening is due to a strong increase of the comoving frame synchrotron emissivity in a relatively thin shell near the outer edge of the visible jet as result of a concentration of magnetic flux at the interface between the relativistic outflow and the non-relativistic disk-wind, i.e. the environment. In contrast to other models limb-brightening here is not an immediate result of deboosted emission in a slow moving sheath; in fact the 'sheath' in our models typically moves slightly faster than the jet body.

The optical knot HST-1 has received much attention. Most MHD models with acceptable fits to the opening angle distribution feature a shock at the distance 70-200 pc. This is particularly true for models with large initial opening angle  $\alpha$ . The shock is due to the fact, that the jet is not in lateral force equilibrium at the launching surface and over-expands. Later, it is forced back towards the axis by magnetic hoop stress and produces a recollimation shock (Bogovalov & Tsinganos 2005). In all cases the shock is visible as a bright spot in the synthetic maps.

We performed our parametric studies unbiased towards the existence of a recollimation shock. All high ranking models have a recollimation shock. Only after ranking our models, we favored for illustrative purposes models with pronounced brightness increase at some point along the axis. We therefore conclude, that the optical bright knot HST-1 is a general feature of all models matching our selection criteria and cannot be seen independently from them. In particular, we suggest, that any physical



model explaining the opening angle and morphological structure will simultaneously also account for HST-1.

In addition our best fitting model is consistent with a number of observational constraints such as the magnetic field in the knot HST-1, and the jet-to-counterjet brightness ratio.

The authors thank the anonymous referee for helping us realize that our model also predicts an essentially one sided jet as observed, Y. Y. Kovalev for providing helpful information on the M87 inner jet structure prior to publication, and S. Jester for fruitful discussion of the

manuscript. Part of this work was supported by the European Community's Research Training Network RTN ENIGMA under contract HPRN-CY-2002-00231 and by the European Community's Marie Curie Actions - Human Resource and Mobility within the JETSET (Jet Simulations, Experiments and Theory) network under contract MRTN-CT-2004 005592. I. A. acknowledges support by the "Spanish Consejo Superior de Investigaciones Científicas" through an I3P contract and the "Ministerio de Ciencia e Innovación" and the European fund for Regional Development through grant AYA2007-67627-C03-03.

#### REFERENCES

- Aloy, M.-A., Gómez, J.-L., Ibáñez, J.-M., Martí, J.-M., & Müller, E. 2000, *ApJ*, 528, L85
- Asada, K., Inoue, M., Nakamura, M., Kamenno, S., & Nagai, H. 2008, *ApJ*, 682, 798
- Asada, K., Inoue, M., Uchida, Y., Kamenno, S., Fujisawa, K., Iguchi, S., & Mutoh, M. 2002, *PASJ*, 54, L39
- Biretta, J. A. 1996, in *Solar and Astrophysical MHD Flows*, ed. K. Tsinganos (Kluwer Academics), 357
- Biretta, J. A., Junor, W., & Livio, M. 2002, *New Astronomy Review*, 46, 239
- Biretta, J. A., Sparks, W. B., & Macchetto, F. 1999, *ApJ*, 520, 621
- Blandford, R. D., & Payne, D. G. 1982, *MNRAS*, 199, 883
- Bogovalov, S., & Tsinganos, K. 1999, *MNRAS*, 305, 211
- . 2005, *MNRAS*, 357, 918
- Bogovalov, S. V. 2001, *A&A*, 371, 1155
- Cheung, C. C., Harris, D. E., & Stawarz, L. 2007, *ApJ*, 663, L65
- Curtis, H. D. 1918, *Publications of Lick Observatory*, 13, 31
- Fendt, C., & Memola, E. 2001, *A&A*, 365, 631
- Gabuzda, D. C., Murray, É., & Cronin, P. 2004, *MNRAS*, 351, L89
- Ghisellini, G., Tavecchio, F., & Chiaberge, M. 2005, *A&A*, 432, 401
- Gómez, J. L., Marscher, A. P., Jorstad, S. G., Agudo, I., & Roca-Sogorb, M. 2008, *ApJ*, 681, L69
- Gracia, J., Peitz, J., Keller, C., & Camenzind, M. 2003, *MNRAS*, 344, 468
- Gracia, J., Tsinganos, K., & Bogovalov, S. V. 2005, *A&A*, 442, L7
- Harris, D. E., Biretta, J. A., Junor, W., Perlman, E. S., Sparks, W. B., & Wilson, A. S. 2003, *ApJ*, 586, L41
- Komissarov, S. S., Barkov, M. V., Vlahakis, N., & Königl, A. 2007, *MNRAS*, 380, 51
- Kovalev, Y. Y. 2008, in *Astronomical Society of the Pacific Conference Series*, Vol. 386, *Extragalactic Jets: Theory and Observation from Radio to Gamma Ray*, ed. T. A. Rector & D. S. De Young, 155+
- Kovalev, Y. Y., Lister, M. L., Homan, D. C., & Kellermann, K. I. 2007, *ApJ*, 668, L27
- Krichbaum, T. P., Lee, S. S., Lobanov, A. P., Marscher, A. P., & Gurwell, M. A. 2008, in *Astronomical Society of the Pacific Conference Series*, Vol. 386, *Extragalactic Jets: Theory and Observation from Radio to Gamma Ray*, ed. T. A. Rector & D. S. De Young, 186+
- Laing, R. A. 1981, *ApJ*, 248, 87
- Ly, C., Walker, R. C., & Junor, W. 2007, *ApJ*, 660, 200
- Macri, L. M., Huchra, J. P., Stetson, P. B., Silbermann, N. A., Freedman, W. L., Kennicutt, R. C., Mould, J. R., Madore, B. F., Bresolin, F., Ferrarese, L., Ford, H. C., Graham, J. A., Gibson, B. K., Han, M., Harding, P., Hill, R. J., Hoessel, J. G., Hughes, S. M. G., Kelson, D. D., Illingworth, G. D., Phelps, R. L., Prosser, C. F., Rawson, D. M., Saha, A., Sakai, S., & Turner, A. 1999, *ApJ*, 521, 155
- Narayan, R., & Yi, I. 1994, *ApJ*, 428, L13
- Owen, F. N., Hardee, P. E., & Cornwell, T. J. 1989, *ApJ*, 340, 698
- Pacholczyk, A. G. 1970, *Radio astrophysics. Nonthermal processes in galactic and extragalactic sources* (Series of Books in Astronomy and Astrophysics, San Francisco: Freeman, 1970)
- Peitz, J., & Appl, S. 1997, *MNRAS*, 286, 681
- Reid, M. J., Biretta, J. A., Junor, W., Muxlow, T. W. B., & Spencer, R. E. 1989, *ApJ*, 336, 112
- Shakura, N. I., & Sunyaev, R. A. 1973, *A&A*, 24, 337
- Tonry, J. L., Dressler, A., Blakeslee, J. P., Ajhar, E. A., Fletcher, A. B., Luppino, G. A., Metzger, M. R., & Moore, C. B. 2001, *ApJ*, 546, 681
- Tsinganos, K., & Bogovalov, S. 2000, *A&A*, 356, 989
- . 2002, *MNRAS*, 337, 553
- Tsinganos, K., & Bogovalov, S. 2005, in *AIP Conf. Proc.* 745: *High Energy Gamma-Ray Astronomy*, 148–159
- Vlahakis, N., & Königl, A. 2004, *ApJ*, 605, 656
- Walker, R. C., Ly, C., Junor, W., & Hardee, P. E. 2008, *ArXiv e-prints*, 803
- Whitmore, B. C., Sparks, W. B., Lucas, R. A., Macchetto, F. D., & Biretta, J. A. 1995, *ApJ*, 454, L73+
- Zavala, R. T., & Taylor, G. B. 2005, *ApJ*, 626, L73